Asian Journal of Pharmaceutical Sciences 17 (2022) 892–907

Available online at www.sciencedirect.com

ScienceDirect

journal homepage: www.elsevier.com/locate/AJPS

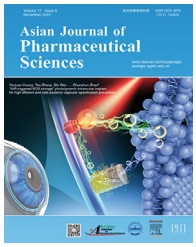

Original Research Paper

A self-guidance biological hybrid drug delivery system driven by anaerobes to inhibit the proliferation and metastasis of colon cancer

Huijuan Zhang[a,b,c], *Yaping Wang*[a], *Mengting Li*[a], *Kexuan Cao*[a], *Zijun Qi*[a], *Ling Zhu*[a,b,c,*], *Zhenzhong Zhang*[a,b,c,*], *Lin Hou*[a,b,c,*]

[a] *School of Pharmaceutical Sciences, Zhengzhou University, Zhengzhou 450001, China*
[b] *Key Laboratory of Targeting Therapy and Diagnosis for Critical Diseases, Zhengzhou 450000, China*
[c] *Collaborative Innovation Center of New Drug Research and Safety Evaluation, Zhengzhou 450000, China*

ARTICLE INFO

Article history:
Received 28 March 2022
Revised 17 July 2022
Accepted 14 September 2022
Available online 19 October 2022

Keywords:
Bifidobacterium Infantis
Hypoxia targeting
TME-responsive drug release
Comprehensive treatment
Colon tumor

ABSTRACT

Colorectal cancer is often accompanied by multiple organ metastasis. Anaerobic *Bifidobacterium Infantis* (BI) bacterial can selectively grow in hypoxic colorectal tumor microenvironment (TME), to own the natural advantage of preferentially colorectal tumor targeting. Herein, a self-guidance biological hybrid drug delivery system (BI-ES-FeAlg/DOX) based on BI was constructed to inhibit the proliferation and metastasis of colon cancer. Results demonstrated that BI-ES-FeAlg/DOX could overcome physical barriers to target and accumulate in colon tumor tissues. Then DOX was released to kill tumor cells along with the phase transition (solid to liquid) of FeAlg hydrogel, due to Fe^{3+} was reduced to Fe^{2+} by intracellular GSH. Meanwhile, BI-ES selectively colonized into tumors and expressed endostatin (ES) protein to down-regulate VEGF and bFGF expression, exerting anti-angiogenic effect. Moreover, FeAlg catalyzed H_2O_2 in the local tumor to generate cytotoxic ·OH, further enhancing the antitumor effect. The pharmacodynamic result in AOM/DSS model proved that BI-ES-FeAlg/DOX had the best therapeutic effect, with the final V/V_0 of 2.19 ± 0.57, which was significantly lower than the other groups. Meanwhile, on CT-26 tumor-bearing model, it also showed an outstanding anti-tumor effect with inhibition rate of $82.12\% \pm 3.08\%$. In addition, lung metastases decreased significantly in tumor metastasis model after BI-ES-FeAlg/DOX treatment.

* Corresponding authors.
E-mail addresses: zhuling1975@zzu.edu.cn (L. Zhu), zhangzz08@126.com (Z.Z. Zhang), houlin_pharm@163.com (L. Hou).
Peer review under responsibility of Shenyang Pharmaceutical University.

https://doi.org/10.1016/j.ajps.2022.09.003

1. Introduction

Cancer is a major disease that seriously threatens people's lives and health. Among them, the incidence and mortality of colorectal cancer ranked third and second, respectively [1]. Colorectal cancer is often accompanied by multiple organ metastasis, such as liver and lung metastasis [2–4]. Currently chemotherapy is still the main clinical treatment method to inhibit the proliferation and metastasis of colorectal cancer [5,6]. However, it can lead to serious systemic side effects because of the poor tumor specificity of chemotherapy drugs [7,8]. In recent years, various micro or nano scale carriers have been developed for the delivery of antitumor drugs. However, most drug delivery systems (DDS) are still unable to achieve effective treatment of colorectal cancer, because the hindrance of tumor matrix makes few drugs actually reach the tumor cells [9]. Therefore, it is of great significance to explore new DDS to overcome the biological transport barriers and deliver sufficient drugs to tumor cells.

At present, the microorganisms used for anti-tumor therapy mainly include viruses and bacteria. The most common viruses are oncolytic viruses, which are mainly administered intratumorally. Although intratumoral delivery of oncolytic viruses can kill the host tumor cells, it has great limitations in clinical application [10]. A variety of anaerobic bacterial have demonstrated their special self-targeting properties for hypoxic tumors [11]. They can overcome the physiological barriers and selectively grow in tumors. Therefore, anaerobic bacterial can be used as a new type of biological carrier for drug delivery and tumor treatment [12,13]. Among them, *Bifidobacterium Infantis* (BI) is one of the most studied and applied strain at present. It was found that after intravenous injection, BI was mainly concentrated in the hypoxic core area of tumor. At the same time, as a common intestinal flora, BI has high biosafety and can live in harmony with the host [14–16]. In addition, BI bacteria are easy to cultured and genetically modify [17–20]. Therefore, the application of BI has promising potential to be a controllable targeted drug delivery platform for multi-mechanism therapy of tumors.

The "tumor gene missile" prepared by genetic engineering technology that based on anti-angiogenesis strategy can search for and kill tumor cells purposefully [21–24]. As an endogenous angiogenesis inhibitor, endostatin (ES) can block tumor angiogenesis by competing with vascular endothelial growth factor (VEGF) and basic fibroblast growth factor (bFGF), thereby inhibit the proliferation and metastasis of colorectal tumor [25–28]. At the same time, the destruction of intratumoral blood vessels aggravates tumor hypoxia, which is more conducive to the colonization of anaerobes in tumor tissue and improve its oncolytic effect [20,29]. Therefore, using anaerobes, such as BI, as gene carriers for ES delivery can complement and promote each other.

Furthermore, studies have shown that doxorubicin (DOX) can enhance the anti-angiogenic effect of ES by inhibiting endothelial cell proliferation and down-regulating VEGF expression. The combined application of DOX and ES can synergistically inhibit the proliferation and metastasis of colorectal cancer [30,31]. However, as an antibiotic chemotherapeutic drug, it will have toxicity to bacteria. Therefore, how to maintain BI activity when using BI as a carrier to deliver DOX, while release DOX at the targeted tumor. Our group prepared nano-sized iron alginate (FeAlg) gel for the first time. It was found that in tumor microenvironment (TME) with low pH and high levels of glutathione (GSH), Fe^{3+} could be reduced to Fe^{2+} and FeAlg carrier changed from gel to sol to release drugs at a fixed point [32,33]. Taking advantage of this property, we intended to synthesize FeAlg gel coated BI to deliver DOX.

Based on the above introduction, an innovative ES and DOX co-delivery biological drug delivery system driven by anaerobes BI was designed as Fig. 1 shown. First of all, the synthesized plasmid carrying ES gene was transfected into BI through electroporation technology, to obtain the transgenic engineering strain BI-ES. Then DOX loaded FeAlg gel was coated onto the surface of BI-ES by electrostatic adsorption to obtain final delivery system BI-ES-FeAlg/DOX. *In vivo*, BI-ES-FeAlg/DOX can actively seek and locate in hypoxic region of colorectal tumor with its hypoxic biological tendency. Then DOX was released to kill tumor cells along with the phase transition (gel→sol) of FeAlg coating, due to Fe^{3+} was reduced to Fe^{2+} by abundant GSH. Moreover, Fe^{2+} catalyzed H_2O_2 in the local tumor to generate cytotoxic •OH, further enhancing the antitumor effect. Meanwhile, due to the colonization and growth of BI-ES in hypoxic tumor, ES gene was overexpressed and cooperated with DOX to block tumor angiogenesis and then play a role in anti-metastasis.

2. Materials and methods

2.1. Materials

DOX and GSH were bought from Beijing Biotopped Technology Co. Ltd (Beijing, China). Sodium alginate (Alg, MW = 200 kDa) was purchased from Huaxi Freda Biomedical Co. Ltd (Shandong, China). $FeCl_3{\cdot}6H_2O$ was supplied by Shanghai Aladdin Biochemical Technology Co. Ltd (Shanghai, China). RPMI 1640 and BI medium was purchased from Beijing Solarbio Science Technology Co., Ltd (Beijing, China). Anti-VEGF, anti-FGF2 and COL18A1 antibodies were obtained from Affinity Biosciences. LTD (Cincinnati, USA). Mouse bFGF and VEGF ELISA kits were purchased from Quanzhou Ruixin Biotechnology Co., Ltd (Quanzhou, China). The pGEX-4T-1-endostatin plasmids and primers were synthesized by Sangon Biotechnology Co., Ltd. (Shanghai, China). PYG liquid medium and TPY agar medium were bought from Qingdao Hope Biotechnology Co., Ltd. (Qingdao, China). *Bifidobacterium Infantis* (BI) strain was purchased from Guangdong Microbial Culture Collection Center (Guangdong, China).

2.2. Growth and bacterial concentration determination of BI

BI was cultured at 37 °C under anaerobic condition for 48 h after inoculating 100 μl BI into 4 ml the liquid PYG medium. After collection by centrifugation at 3000 rpm for 5 min, BI were resuspended with sterile saline to an optical density

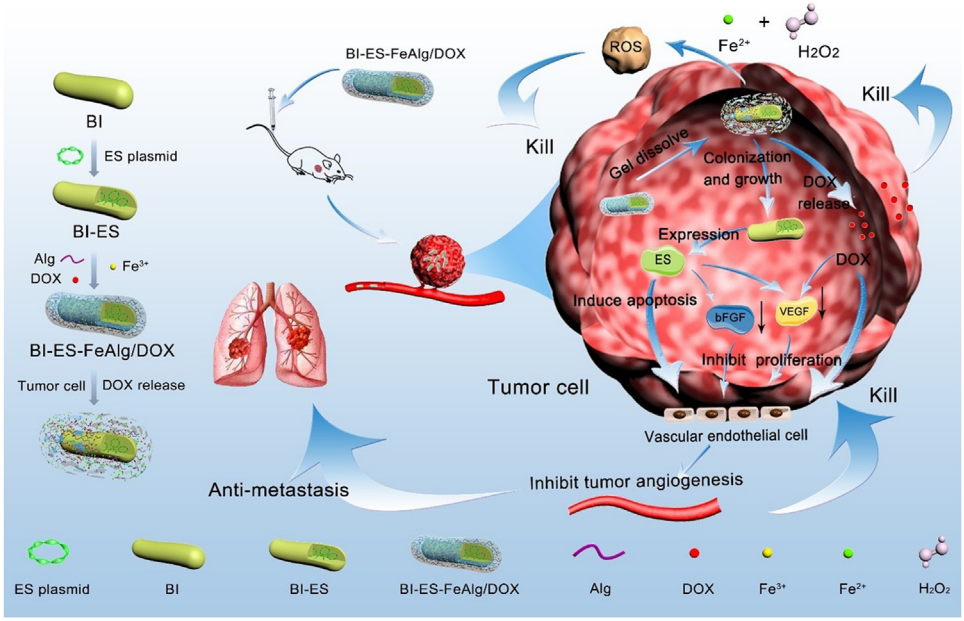

Fig. 1 – Schematic illustration of the synthesis process and mechanism of BI-ES-FeAlg/DOX.

(OD_{600}) of 0.15, corresponding to a bacterial concentration of 3×10^8 CFU/ml. Serially diluting the bacterial suspension and counting CFUs under the microscope to determine bacterial concentration.

2.3. *Synthesis of BI-ES*

Electrocompetent cells of BI were prepared according to the method reported by Rossi et al. [34]. Then pGEX-4T-1-endostatin plasmids (ES expression vector) were transfected directly into BI by electroporation in a Bio-Rad Gene-Pulser apparatus at 25 μF and 2.5 kV with the pulse controller set at 200 Ω. Transfected BI was grown on TPY agar plates containing 20 μg/ml ampicillin (Amp). After 72 h of incubation at 37 °C under anaerobic condition, stable BI-ES with Amp resistance was selected and confirmed by PCR technology.

2.4. *Preparation of BI-ES-FeALg/DOX*

First, DOX (5.4 mg) and Alg (1.8 mg) were added in 24.0 ml PBS and magnetically stirred for 24 h at 25 °C. Thereafter, 1 ml BI-ES suspension (4.5×10^8 CFU/ml) was added and kept stirring for 30 min. Finally, 6 ml $FeCl_3 \cdot 6H_2O$ solution (0.8 mg/ml) was dropped into the mixture (1 ml/min). After further stirring for 3 h, BI-ES-FeAlg/DOX can be easily obtained by centrifugation at 4 °C (3000 rpm, 5 min).

2.5. *Characterization of BI-ES-FeALg/DOX*

The morphology of pure BI and BI-ES-FeAlg/DOX were characterized by TEM (TF20, JEOL 2100F) and SEM (Apreo 2, FEI). The particle size and zeta potential were analyzed by Nano laser particle size analyzer (Zetasizer Nano ZS-90, Malvern). The spectral characteristics were examined by UV-visible spectrophotometer (UV-2250, Shimadzu).

2.6. *Growth characteristics of BI-ES-FeALg/DOX in vitro*

BI, BI-ES, BI-ES-FeAlg and BI-ES-FeAlg/DOX were inoculated into fresh PYG medium and cultured at 37 °C under anaerobic condition, respectively. Then the OD_{600} values of each group were measured at 0, 8, 12, 16, 20, 24, 32, 36 and 40 h. Take the culture time and OD_{600} value as abscissa and ordinate to draw bacterial growth curve.

BI-ES and BI-ES-FeAlg/DOX were inoculated into the serum of mice and cultured at 37 °C under anaerobic condition, respectively. Then the OD_{600} values of each group were measured at 0, 8, 12, 16, 20, 24, 32, 36 and 40 h. Take the culture time and OD_{600} value as abscissa and ordinate to draw the bacterial growth curve.

2.7. *Determination of drug loading and encapsulation efficiency*

To determine the encapsulation efficiency of BI-ES-FeAlg/DOX, the supernatant of BI-ES-FeAlg/DOX prepared as above was collected after centrifugation. Thereafter, unloaded DOX in supernatant was measured through a UV-visible spectrophotometer at 481 nm. The loaded DOX can be calculated by (Total amount of DOX added – unloaded DOX), and then drug encapsulation efficiency can be calculated using the following Eq. 1. For determination of drug loading efficiency, we measured the mass of BI-ES-FeAlg/DOX precipitate and calculated using the following Eq. 2:

$$\text{Encapsulationefficiency}\,(\%) = \frac{W_{\text{Loaded DOX}}}{W_{\text{DOX added initially}}} \times 100\% \quad (1)$$

$$\text{Loadingefficiency}\,(\%) = \frac{W_{\text{Loaded DOX}}}{W_{\text{BI-ES-FeAlg/DOX}}} \times 100\% \quad (2)$$

2.8. Evaluation of drug release property

In brief, BI-ES-FeAlg/DOX was sealed into dialysis bags (MW=3500 Da) and immersed in 40 ml the following PBS buffer (① pH 7.4; ② pH 5.5; ③ pH 6.5; ④ 5 mM GSH; ⑤ 20 μM GSH; ⑥ pH 5.5 and 5 mM GSH; ⑦ pH 6.5 and 20 μM GSH). Put the above medium in an incubator shaker and shake immediately at 37 °C with the rotating speed of 100 rpm. At the pre-set time, take out 1 mL of samples to measure DOX release amount.

2.9. Invasion and drug delivery capacity of BI-ES-FeALg/DOX in CT-26 cells

Firstly, the capacity of BI bacteria to invade CT-26 cells was investigated. Briefly, CT-26 cells in 12-well plates were treated with BI-ES, BI-ES-FeAlg or BI-ES-FeAlg/DOX (BI-ES: 2×10^8 CFU/ml) for 1, 2 and 4 h, respectively. After that, plates were washed twice with sterile PBS. After digestion and centrifugation (1000 rpm, 5 min), cells were collected, washed twice by centrifugation, mixed with 0.1% Triton X-100, and strongly agitated. Next, the precipitate was collected by centrifugation, plated into PYG liquid medium, and cultured at 37 °C under anaerobic condition for 48 h. Finally, OD600 values of each culture medium were measured using the UV-visible spectrophotometer, to calculate the bacteria concentration.

Secondly, the drug delivery ability of BI-ES-FeAlg/DOX in CT-26 cells was studied using flow cytometer. In brief, CT-26 cells were incubated in 6-well plates for 24 h, and then treated with BI-ES-FeAlg/DOX and FeAlg/DOX (DOX: 2 μg/ml) for 1, 2 and 4 h, respectively. Thereafter, cells were washed and collected for flow cytometer determination.

2.10. The capacity of macrophages to uptake BI-ES-FeAlg /DOX

The uptake capacity of BI-ES-FeAlg /DOX by macrophages was studied using flow cytometer. In brief, macrophages were incubated in 6-well plates for 24 h, and then treated with BI-ES-FeAlg/DOX (DOX: 2 μg/ml) for 1, 2 and 4 h. Thereafter, macrophages were washed and collected for flow cytometer determination.

2.11. Cytotoxicity

CT-26 cells were seeded in 96-well plates at a density of 6×10^3 cells per well and incubated for 24 h. Then cells were treated with DOX, FeAlg, FeAlg/DOX, BI-ES-FeAlg and BI-ES-FeAlg/DOX, respectively. The concentrations of DOX in above formulations were 0.5, 1, 2, 5 and 10 μg/ml. After further incubation for 24 or 48 h, cell viability was measured by SRB assay.

2.12. Intracellular •OH determination

Briefly, CT-26 cells in 6-well plates were treated with 0.5, 2 and 4 μg/ml of FeAlg for 2 h and then incubated with 10 μM of DCFH-DA probe for 30 min in dark. After that, cells were washed and fixed with 800 μl ice ethanol for 2 min. Finally, the green fluorescence was observed under a fluorescence microscope.

2.13. Tumor deep penetration in vitro

The three-dimensional multicellular sphere (3DMCS) model was established using CT-26 cells to evaluate tumor deep penetration ability of BI-ES-FeAlg. In brief, CT-26 cells were incubated in the low-adsorption culture plate (8×10^3 cells/well) for one week to obtain a 3DMCS model. Then The spheres were treated with DOX, FeAlg/DOX and BI-ES-FeAlg/DOX for 12 h (DOX: 2 μg/ml). After washing with PBS, the red fluorescence of DOX was observed and recorded using LSCM. Moreover, the fluorescence intensity of DOX at different depths from the top of 3DMCS was measured by ImageJ software.

2.14. Determination of ES, VEGF and bFGF expression

Western blot analysis was used to determine intracellular expression of ES, VEGF and bFGF. Briefly, CT-26 cells were incubated with DOX, BI-ES-FeAlg, BI-ES-FeAlg/DOX (DOX: 2 μg/ml) for 24 h. After lysis with RIPA lysate buffer, CT-26 cells were centrifuged at 4 °C (12 000 rpm, 15 min). Subsequently, the supernatant was collected for measuring the expression level of ES, VEGF and bFGF *via* standard western blotting procedures.

2.15. Wound healing migration assay

Wound healing migration assay was used to detect the migration ability of CT-26 tumor cells after BI-ES-FeAlg/DOX treatment. Briefly, CT-26 cells were seeded in 6-well plates and cultured for 24 h. Thereafter, cell monolayers were carefully wounded with a 10 μl pipette tip, and further incubated with drug-containing serum-free medium. The experiment was divided into DOX, BI-ES-FeAlg and BI-ES-FeAlg/DOX three groups (DOX: 2 μg/ml). Cell treated with serum-free medium was used as the control group. Images of wound areas were recorded at 0, 12 and 24 h using an inverted microscope (Zeiss LSM 510). Gap distance of the wound was analyzed using ImageJ software. Migration rate was calculated by the Eq. 3:

$$\text{Migration rate} = [(\text{Scratch width at 0 h} - \text{Scratch width at pre-set time point}) / \text{Scratch width at 0 h}] \times 100\% \quad (3)$$

2.16. Transwell experiment

Transwell experiment was used to evaluate the effect on tumor cell invasion and metastasis ability. CT-26 cells were seeded into the upper transwell chamber pre-coated with matrigel, and incubated with serum-free medium containing drugs (DOX, BI-ES-FeAlg and BI-ES-FeAlg/DOX). 10% FBS-containing medium was added to the lower chamber. 24 h later, unmigrated cells were wiped from the upper side of the membrane. The migration cells in lower surface were observed and recorded using the microscope after staining by 0.1% crystal violet. Furthermore, dissolve those stained tumor cells in 35% acetic acid and measure the absorbance at 560 nm, to calculate the invasion and metastasis ability using the Eq. 4:

Invasion ability
$$= OD_{560} \text{ of treatmentgroup} / OD_{560} \text{ of control group} \quad (4)$$

2.17. Animals

BALB/c mice (6 − 8 weeks old, 18−20 g) were obtained from Hunan SJA Laboratory Animal Co., Ltd. (Hunan, China). All animal procedures were performed in accordance with the Guidelines for Care and Use of Laboratory Animals of Zhengzhou University (syxk 2018–0004).

2.18. The AOM/DSS induced orthotopic colon cancer model establishment

To establish the AOM/DSS-induced orthotopic colon cancer model, BALB/c mice were injected intraperitoneally with AOM solution (10 mg/kg) firstly. One week later, mice were given 2.5% DSS dissolving in drinking water for 7 d, followed by substitution of regular water for 14 d. After that, mice were subjected to more than 2 cycles of 2.5% DSS treatment (7 d/cycle). This orthotopic colon cancer mouse model was successfully established at the end of the eighth week. During this period, disease activity index (the sum of body weight, diarrhea degree and bleeding degree in the rectum) were determined every 4 d. Body weight was scored 0, 1, 2, 3 and 4 for 0, 1%−5%, 6%−10%, 11%−15% and >15% body weight loss, respectively. Diarrhea degree was scored 0, 1, 2, 3 and 4 for well-formed pellets, soft pellets, pasty stools, liquid stools and diarrhea, respectively. Bleeding degree was scored 0, 1, 2 and 3 for no bleeding, occult bleeding, slight bleeding and gross bleeding, respectively. In addition, at the 0, 7th, 28th, 49th, 56th d, the colon of mice was fetched out to measure the length and check the pathological changes by hematoxylin and eosin (H&E) staining.

2.19. Biodistribution study

To evaluate targeting, IR783-labeled FeAlg and BI-ES-FeAlg were intravenously injected into the AOM/DSS model mice with the same dosage of IR783 (2 mg/kg). At 1, 2, 4, 6, 12, 24 and 36 h after administration, the fluorescence distribution and intensity of IR783 was measured using FX PRO *in vivo* imaging system. Furthermore, the mice were euthanized and heart, liver, spleen, lung, kidney and colon tissues in each group were dissected at 36 h for *ex vivo* imaging. Normalized fluorescence intensity was calculated using ImageJ software.

2.20. The tendency to hypoxic core area of tumor

DOX, FeAlg/DOX and BI-ES-FeAlg/DOX (DOX: 2 mg/kg) were intravenously administered to AOM/DSS model mice, respectively. 18 h post-injection, the mice were sacrificed and the colon tumor tissues were taken out. The nucleus and hypoxic area were stained with DAPI (blue) and FITC-labeled HIF-1a (green) antibody, respectively.

2.21. Antitumor efficacy

36 AOM/DSS model mice with similar body weights were randomly divided into 6 groups and treated respectively with PBS (Control), DOX, FeAlg, FeAlg/DOX, BI-ES-FeAlg and BI-ES-FeAlg/DOX (DOX: 2 mg/kg) via intravenous administration every 2 d (10 times in total). The disease activity index was calculated and recorded according to the above method. At the end of the antitumor effect study, blood samples of mice were collected to measure the blood routine index (WBC, RBC, HGB and PLT). The mice were sacrificed and colon tissues were fetched out. After being cleaned with PBS to remove the residual feces, the colon was cut along the midline and spread out, to count the number of tumors and measure the long diameter A and short diameter B of tumors. Finally, calculate the tumor load (the sum of all tumor volumes) according to the following Eq. 5. In order to observe the histopathological changes, heart, liver, spleen, lung, kidney and colon tissues of each group were collected to calculate viscera coefficient, as well as H&E analysis. Furthermore, colon tumor tissues were collected for PE-CD31 immunofluorescence staining to evaluate the tumor vascular density.

$$\text{Tumor load} = \text{Sum}\ (A \times B^2/2) \quad (5)$$

2.22. In situ •OH produced by FeALg

Because FeAlg can catalyze H_2O_2 to generate •OH in tumor tissue to enhance the antitumor efficacy of BI-ES-FeAlg/DOX, we determined *in situ* •OH level using ROS fluorescent probe-DHE. AOM/DSS model mice were treated respectively with PBS (Control) and FeAlg *via* intravenous administration. 12 h post-injection, the mice were sacrificed and the colon tumor tissues were taken out. After washing with PBS, tumor frozen sections (10 μm) were prepared and stained with DHE probe. The fluorescence microscope was used to record results. Normalized fluorescence intensity was calculated using ImageJ software.

2.23. CT-26 tumor-bearing model establishment

BALB/c mice were injected with CT-26 cells (2×10^6) in the right fore limb subcutaneously. When tumors grew to ~100 mm^3, CT-26 tumor-bearing mouse model was successfully constructed and can be used for *in vivo* experiments.

2.24. Biodistribution study and tumor targeting evaluation

IR783-labeled FeAlg and BI-ES-FeAlg were intravenously injected into the CT-26 tumor-bearing model mice with the same dosage of IR783 (2 mg/kg). At 1, 2, 4, 6, 12, 24 and 36 h after administration, the fluorescence distribution and intensity of IR783 was measured using FX PRO *in vivo* imaging system. Furthermore, 36 h post-injection, the major organs and tumor tissues were dissected for *ex vivo* imaging. Normalized fluorescence intensity was calculated using ImageJ software.

2.25. Pharmacokinetic experiments of bacteria

The pharmacokinetic experiments were performed on 6–8-weeks-old BALB/c mice. Briefly, BI-ES and BI-ES-FeAlg/DOX were intravenously injected into BALB/c mice with the same dosage of BI (1×10^7 CFUs). 10 μl blood were collected through

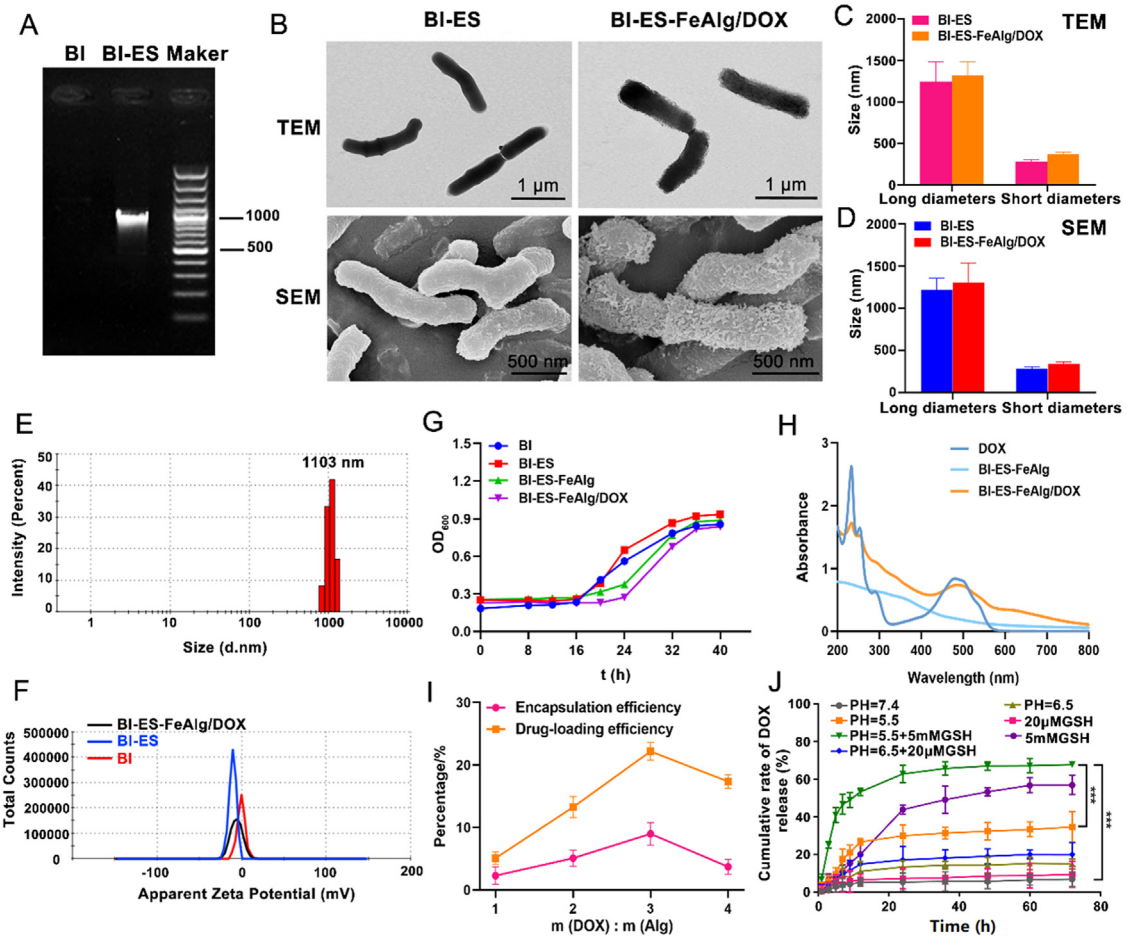

Fig. 2 – Synthesis and characterization of BI-ES-FeAlg/DOX. (A) Identification of ES gene transfected into BI-ES by PCR analysis. (B) The morphological characteristics of BI-ES and BI-ES-FeAlg/DOX observed by TEM and SEM. (C) The long and short diameters of BI-ES and BI-ES-FeAlg/DOX measured from TEM image. (D) The long and short diameters of BI-ES and BI-ES-FeAlg/DOX measured from SEM image. (E) Size distribution of BI-ES-FeAlg/DOX determined by DLS. (F) Zeta potential of BI, BI-ES and BI-ES-FeAlg/DOX. (G) The growth curve of BI, BI-ES, BI-ES-FeAlg and BI-ES-FeAlg/DOX. (H) UV–Vis spectra of DOX, BI-ES-FeAlg and BI-ES-FeAlg/DOX. (I) Drug loading and encapsulation efficiency of DOX in BI-ES-FeAlg/DOX at different feding ratios ($n = 3$). (J) DOX release profile from BI-ES-FeAlg/DOX in different conditions ($n = 3$).

the eye socket at 1, 2, 4, 24 and 36 h post-injection. Each portion of the blood sample was diluted with 90 μl PBS. Thereafter, 50 μl the above dilution was spread on solid TPY agar plates. After incubation at 37 °C for 72 h under anaerobic condition, the colonies on agar plates were counted and recorded.

2.26. *Levels of cytokines in serum*

Briefly, BI-ES and BI-ES-FeAlg/DOX were intravenously injected into BALB/c mice with the same dosage of BI (1×10^7 CFUs). 1 ml blood were collected through the eye socket at 1, 4, 8, 12, 24 and 36 h post-injection. The serum was isolated by centrifugation (3000 rpm, 5 min) and then IL-10 and TNF-α were measured using commercially available ELISA kits.

2.27. *Pharmacodynamic experiment*

36 tumor-bearing mice with similar body weights were randomly divided into 6 groups and treated respectively with PBS (Control), DOX, FeAlg, FeAlg/DOX, BI-ES-FeAlg and BI-ES-FeAlg/DOX (DOX: 2 mg/kg) via intravenous administration every 2 d (10 times in total). The tumor volume was calculated according to the formula $V = (A \times B^2)/2$, where A and B represent the long diameter and short diameter of the tumor, respectively. At the end of the experiment, blood samples of mice were collected to measure the blood routine index (WBC, RBC, HGB and PLT). Finally, mice were sacrificed and tumor tissues were collected as well as weighed, to calculate tumor inhibition rate according to the following Eq. 6, in which W represented the average tumor weight. In order to observe the histopathological changes, heart, liver, spleen, lung, kidney and tumor tissues of each group were stained with (H&E).

$$\text{Tumor inhibition rate (\%)} = \frac{W_{\text{control group}} - W_{\text{experimental group}}}{W_{\text{control group}}} \times 100\% \quad (6)$$

2.28. Lung metastasis model

In order to evaluate the antitumor metastasis effect, we constructed lung metastasis model. Briefly, BALB/c mice were injected with CT-26 cells (5×10^5) *via* the tail vein. At the 5th d, 36 lung metastasis model mice with similar body weights were randomly divided into 6 groups and treated respectively with PBS (Control), DOX, FeAlg, FeAlg/DOX, BI-ES-FeAlg and BI-ES-FeAlg/DOX (DOX: 2 mg/kg) via intravenous administration every 2 d (5 times in total). The body weight was measured before administration. At the end of the experiment, the lung tissues were isolated to visually observe lung metastatic pulmonary nodules. H&E staining was also used to observe the histopathological changes and evaluate the pulmonary metastasis of CT-26 tumor. Moreover, the lung tissues in Control, DOX, BI-ES-FeAlg and BI-ES-FeAlg/DOX groups were homogenized to determine bFGF and VEGF expression using ELISA analysis method.

2.29. Statistical analysis

Data were analyzed using GraphPad Prism8 software (Diego, USA). p-Values less than 0.05 were considered statistically significance ($^*P < 0.05$, $^{**}P < 0.01$, $^{***}P < 0.001$).

3. Results and discussion

3.1. Synthesis and characterization of BI-ES-FeALg/DOX

The pGEX-4T-1-endostatin plasmids transfected into BI-ES were proved by PCR technology. As Fig. 2A shown, the ~1000 bp band appeared in BI-ES group while not in BI negative control group, indicating that ES gene was transfected into BI successfully.

Next, BI-ES-FeAlg/DOX delivery system was prepared by a one-step titration method. TEM and SEM images showed the morphology of BI-ES and BI-ES-FeAlg/DOX. As seen in Fig. 2B, BI-ES exhibited a typical rod shape and smooth surface, with the long and short diameters of ~1.2 μm and ~280 nm, respectively (Fig. 2C-2D). After coated with gels, BI-ES-FeAlg/DOX demonstrated a rough surface and increased long and short diameters of ~1.3 μm and ~350 nm, respectively. The hydrodynamic particle size of BI-ES-FeAlg/DOX increased from 944 nm to 1103 nm with PDI of 0.281 (Figs. 2E and S1), which also proved the successful coating of FeAlg/DOX hydrogel. Fig. S2 further revealed that BI-ES-FeAlg/DOX was red-brown, with good water dispersibility. In addition, Fig. 2F demonstrated that the zeta potential of BI-ES-FeAlg/DOX was negative (−10.8 mV). We also checked whether the drug-loaded FeAlg hydrogel coating would compromise the activity of BI to replicate. The OD_{600} value had a linear positive correlation with the number of BI bacteria (Fig. S3). Therefore, we evaluated the replication ability of BI before and after coating by measuring the OD_{600} of the bacterial culture medium. As Figs. 2G and S4 shown, BI-ES-FeAlg and BI-ES-FeAlg/DOX had the similar growth profile. From 18 to 32 h, the OD values of BI-ES-FeAlg/DOX were slightly lower than that of BI-ES. This may be due to the formation of FeAlg gel layer. The FeAlg hydrogel coating on the surface of BI-ES can hinder the nutrient contact between BI bacteria and the external medium to a certain extent, so that some proteins, inorganic salts, etc. necessary for bacterial growth cannot be quickly supplied. Therefore, the growth rate of BI bacteria with hydrogel coating will be affected to a certain extent in the early stage.

DOX had a typical UV–vis absorption peak at 481 nm (Fig. S5). After DOX-loaded FeAlg hydrogel coating, there was an apparent peak appeared at around 481 nm, as shown in Fig. 2H. Based on the standard curve of DOX at 481 nm (Fig. S6), the drug loading and encapsulation efficiency of DOX were determined to select the optimal feeding weight ratio. As shown in Fig. 2I, the feeding ratio of 3:1 (DOX: Alg) was the optimal prescription condition, with the highest drug loading and encapsulation efficiency of 22.19% and 8.99%, respectively.

3.2. In vitro TME-responsive drug release profile

The TME-responsive drug release experiment of BI-ES-FeAlg/DOX was carried out *in vitro* to investigate the fixed-point release profile of DOX. Because TME is a weakly acidic and highly reductive environment, the drug release behavior of BI-ES-FeAlg/DOX was studied in PBS buffer with different pH values and GSH concentrations. As Fig. 2J shown, there was only 6.83% of DOX released from BI-ES-FeAlg/DOX in pH 7.4 medium, confirming the protective effect of FeAlg hydrogel. In comparison, in pH 5.5 and GSH (5 mM) medium, the cumulative release percentages of DOX increased by ~28% and ~50%, respectively, revealing the pH and GSH sensitivity. Moreover, in the simulated tumor cells environment (pH 5.5 + 5 mM GSH), drug release amount from BI-ES-FeAlg/DOX reached as high as 67.72%, which was much higher than the other groups. On the one hand, this may because H^+ ions can compete with Fe^{3+} ions for carboxyl group binding site of sodium alginate, resulting in depolymerization of the FeAlg hydrogel and acid-responsive drug release. On the other hand, this was due to the coordination characteristics of Alg and different iron ions. Fe^{3+} could be reduced to Fe^{2+} owing to the weakly acidic and highly reductive microenvironment. The affinity between Fe^{2+} and Alg decreased, leading to FeAlg gels decomposition along with DOX release.

3.3. Invasion capacity and drug delivery ability of BI-ES-FeALg/DOX in CT-26 cells

Firstly, we investigated whether the coating of FeAlg and FeAlg/DOX hydrogel would compromise the ability of BI-ES to invade tumor cells. As shown in Fig. 3A, with the extension of incubation time, BI-ES invading tumor cells gradually increased. The ability of bacterial invasion was similar after incubating CT-26 cells for 1 h with BI-ES, BI-ES-FeAlg or BI-ES-FeAlg/DOX. With the extension of incubation time, the amount of BI that invaded CT-26 cells increased significantly. This result proved that BI-ES bacteria can easily invade tumor cells, and FeAlg/DOX hydrogel coating did not affect its invasion capacity. Secondly, we quantitatively evaluated the ability of BI-ES bacteria to carry DOX into CT-26 cells by flow cytometry. As seen in Fig. 3B, at 1, 2 and 4 h, the accumulation of DOX in CT-26 cells was 25.8%, 66.0% and 86.1%, respectively. And at each time points, the intake of DOX by CT-26 cells incubation with BI-ES-FeAlg/DOX was

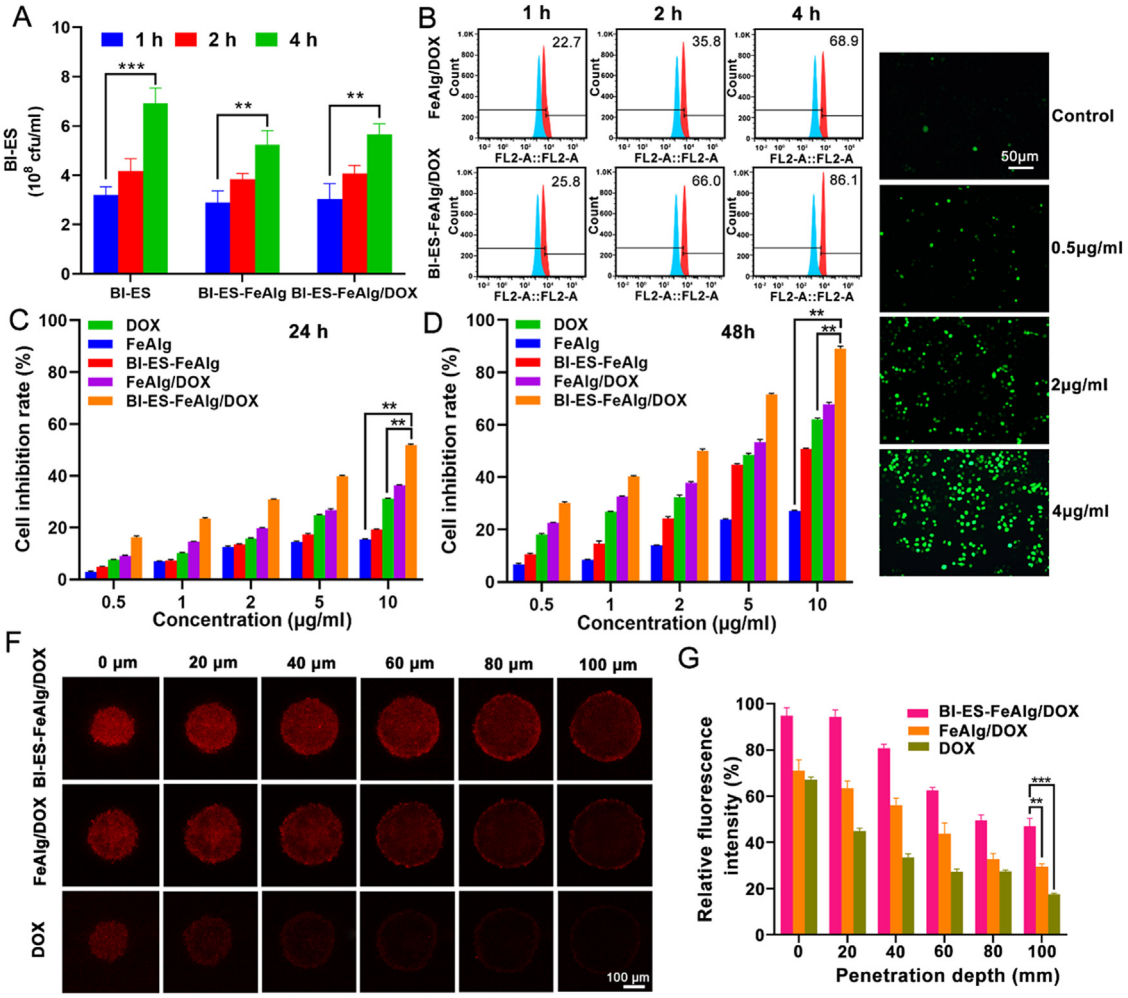

Fig. 3 – Effects of BI-ES-FeAlg/DOX on CT-26 cells *in vitro*. (A) Ability of BI-ES, BI-ES-FeAlg and BI-ES-FeAlg/DOX to invade CT-26 cells during 1, 2 or 4 h incubation. (B) Quantitative determination of intracellular amount of BI-ES-FeAlg/DOX or FeAlg/DOX in CT-26 cells at different time intervals. (C-D) The cytotoxicity results at 24 h and 48 h ($n = 6$). (E) The •OH in CT-26 cells after incubation with 0.5, 2 and 4 μg/mL of FeAlg. (F) The fluorescence image result of CT-26 3DMCS at different depths. (G) The semiquantitative fluorescence analysis result of (F) ($n = 3$).

significantly more than that of FeAlg/DOX group. These results indicated BI-ES could invade and deliver drugs into tumor cells quickly and effectively, to exert superior antitumor efficacy.

3.4. *The capacity of macrophages to uptake BI-ES-FeAlg /DOX*

As shown in Fig. S7, the accumulation amount of BI-ES-FeAlg/DOX in macrophages was 7.23%, 12.4% and 45.8% at 1, 2 and 4 h, respectively. And the uptake capacity of BI-ES-FeAlg/DOX by macrophages was significantly lower than that by tumor cells, suggested that after accumulation in tumor tissue, BI-ES-FeAlg/DOX would be more inclined to be taken up by CT-26 tumor cells, thereby exerting antitumor effect.

3.5. *Cytotoxicity*

Given the promising invasion capacity and drug delivery ability of BI-ES-FeAlg/DOX, the cytotoxicity of BI-ES-FeAlg/DOX to CT-26 tumor cells was determined *in vitro*. As shown in Fig. 3C-3D, cell inhibition rates in all groups demonstrated a concentration and time dependent manner. At 24 h, the cell inhibition rates of FeAlg, BI-ES-FeAlg, DOX, FeAlg/DOX and BI-ES-FeAlg/DOX (10 μg/mL) were 15.47%, 19.25%, 31.17%, 36.33% and 51.85%, respectively. The IC50 values of DOX and BI-ES-FeAlg/DOX were calculated as 15.4 and 8.63 μg/ml at 24 h, respectively. At 48 h, cell inhibition rate of BI-ES-FeAlg/DOX (10 μg/ml) was 89.15%, and the IC50 values of DOX and BI-ES-FeAlg/DOX were calculated as 5.55 and 1.95 μg/ml, respectively. Compared with free DOX, the significantly lower IC50 value of BI-ES-FeAlg/DOX indicated that BI-ES-FeAlg/DOX had an obviously improved anti-tumor effect *in vitro*, owing to the combination tumor killing effect of DOX-based chemotherapy and FeAlg-based ROS therapy. After entering tumor cells, the cross-linking agent $Fe^{3+}$of FeAlg was reduced to Fe^{2+}. On one hand, FeAlg hydrogel coating depolymerized and released DOX to play a chemotherapeutic effect. On the other hand, Fe^{2+} catalyzed H_2O_2 to produce •OH and further killed tumor cells (Fig. 3E).

3.6. *In vitro tumor deep penetration based on the hypoxic biological tendency of Bi*

Next, we explored whether anaerobic BI can overcome the tumor physiological barrier, deliver drugs to the hypoxic tumor central area, and realize the uniform distribution of drugs throughout the tumor tissue. The CT-26 3DMCS model was constructed to simulate tumor tissue *in vivo*. The CT-26 3DMCS was incubated with DOX, FeAlg/DOX and BI-ES-FeAlg/DOX for 12 h, respectively. As shown in Fig. 3F, the fluorescence of DOX mainly distributed in the edge regions of 3DMCS. However, in FeAlg/DOX group, DOX fluorescence was observed in the center of 3DMCS at a depth of 40 μm, owing to the particle size conversion characteristics of FeAlg nanogel [32,33]. Particularly, in BI-ES-FeAlg/DOX group, obvious fluorescence can be seen in the deep region of 3DMCS at a depth of 80 μm. Moreover, Fig. 3G demonstrated that the fluorescence intensity of DOX in BI-ES-FeAlg/DOX group at different depths was all higher than that of the other two groups, indicating that BI-ES could significantly improve the intratumoral distribution behavior of DOX. This may be attributed to two factors: (1) The natural hypoxic biological tendency enables BI-ES to actively migrate to the hypoxic tumor center [12,35]; (2) The TME-responsive particle size conversion feature of DOX-loaded FeAlg coating was conducive to drug delivery to the deep tumor [32,33].

3.7. *Anti-invasion and migration ability of BI-ES-FeALg/DOX on CT-26 cells*

Given that the combined application of DOX and ES can synergistically inhibit the metastasis of colorectal cancer, we evaluated *in vitro* invasion and migration ability of CT-26 cells treated with serum-free medium, DOX, BI-ES-FeAlg and BI-ES-FeAlg/DOX respectively. To confirm the expression of ES gene transferred into CT-26 cells by BI, the expression level of ES was determined by Western blot method. As Fig. 4A-4B shown, no ES protein was detected in blank CT-26 tumor cells, while ES was augmented in BI-ES-based groups, confirming that ES gene can be successfully expressed in tumor cells. Moreover, the bFGF protein level was observed to be downregulated in BI-ES-based groups, suggesting that ES gene can competitively inhibit bFGF expression. In addition, the VEGF level was downregulated in all treatment groups, especially in BI-ES-FeAlg/DOX group, indicating that ES gene and DOX can synergistically inhibit VEGF expression.

As we know, down-regulation of bFGF and VEGF proteins is beneficial to block tumor angiogenesis and inhibit tumor metastasis. Therefore, we further studied the anti-invasion and migration ability of BI-ES-FeAlg/DOX on CT-26 cells *in vitro*. As Fig. 4C-4D shown, at 24 h, the migration rates of CT-26 cells in control, DOX, BI-ES-FeAlg and BI-ES-FeAlg/DOX groups were 60.1% ± 4.29%, 44.4% ± 5.24%, 26.9% ± 3.71% and 18.3% ± 2.72%, respectively. In addition, Fig. 4E-4F showed that CT-26 cells incubated with serum-free medium (Control group) demonstrated the highest invasion and metastasis ability. However, after treatment with BI-ES-FeAlg/DOX for 24 h, the invasion and metastasis ability of CT-26 cells sharply decreased to 0.46 ± 0.03. The above results indicated that BI-ES-FeAlg/DOX delivery system can express ES protein in CT-26 tumor cells, to block angiogenesis and inhibit tumor metastasis by down-regulating bFGF, as well as cooperating with DOX to down-regulate VEGF expression.

3.8. *In vivo study on AOM/DSS-induced orthotopic colon tumor model*

Firstly, we examined the anti-tumor potential of BI-ES-FeAlg/DOX on AOM/DSS-induced orthotopic colon tumor mouse model [36,37]. The disease activity index (DAI) and colon morphology changes during AOM/DSS-induced process (shown in Fig. 5A) were shown in Fig. 5B and S8. The model mice exhibited obviously increased DAI, as well as thickened and shortened colon. Moreover, H&E staining result of colon tissue during the AOM/DSS-induced process was shown in Fig. 5C. On Day 0, the colonic epithelial cells were regularly arranged and the glands were uniformly distributed, without inflammatory cell infiltration. Along with time, extensive infiltration of inflammatory cells and extremely disordered epithelial cells emerged. On Day 56, the proliferative colon tumor cells were spread out diffusely, indicating the successful establishment of the orthotopic colon tumor mouse model.

Then the colon tumor targeting property based on the hypoxic biological tendency of BI was investigated using *in vivo* imaging technology. The result can be seen in Fig. 5D. The colon tumor tissue exhibited relatively weak fluorescence signal in free IR783 group. While in FeAlg/IR783 group, there was stronger fluorescence signal observed in colon sites at 12 h. Particularly, BI-ES-FeAlg/IR783 treated mice exhibited the highest fluorescence signal in colon tumors and remained strong even at 36 h post-injection, indicating that BI-ES-FeAlg/IR783 could accumulate rapidly and massively at tumor tissues. At 36 h, the mice were sacrificed for *ex vivo* imaging. As Fig. 5E-5F demonstrated, BI-ES-FeAlg/IR783 mainly distributed in colon tissues and the fluorescence intensity was much higher than the other two groups, further demonstrating its excellent tumor targeting accumulation capacity. In addition, we explored whether anaerobic BI can overcome the tumor physiological barrier and deliver drugs to the hypoxic tumor central area *in vivo*. The tumor cell nuclei and hypoxic regions were stained with DAPI (blue) and FITC-labeled HIF-1α (green), respectively. As shown in Fig. 5G and S9, BI-ES-FeAlg/IR783 could deliver most DOX to the hypoxic colon tumor sites, with 6-fold higher delivery efficiency than that of free DOX group. What was particularly noticeable was the remarkable colonization characteristics of BI-ES-FeAlg/DOX in tumor hypoxic areas. As Fig. 5G-5H demonstrated, DOX in BI-ES-FeAlg/DOX group appeared only in oxygen-deficient tumor regions with colocalization coefficient of 0.94 ± 0.03, further proving the superiority of BI bacteria as carriers to deliver drugs to hypoxic solid tumors.

Next, we explored the anti-tumor effect of BI-ES-FeAlg/DOX on AOM/DSS-induced mouse model. As Fig. 6A-6B demonstrated, compared with control group, the length of colon in treatment groups increased, and BI-ES-FeAlg/DOX group was the most significant with 26.9% increasement in colon length. Moreover, the longitudinal-section images of colon tissues (Fig. 6C) showed that the tumor-bearing colon tended to be normal with smoother surface after treatment

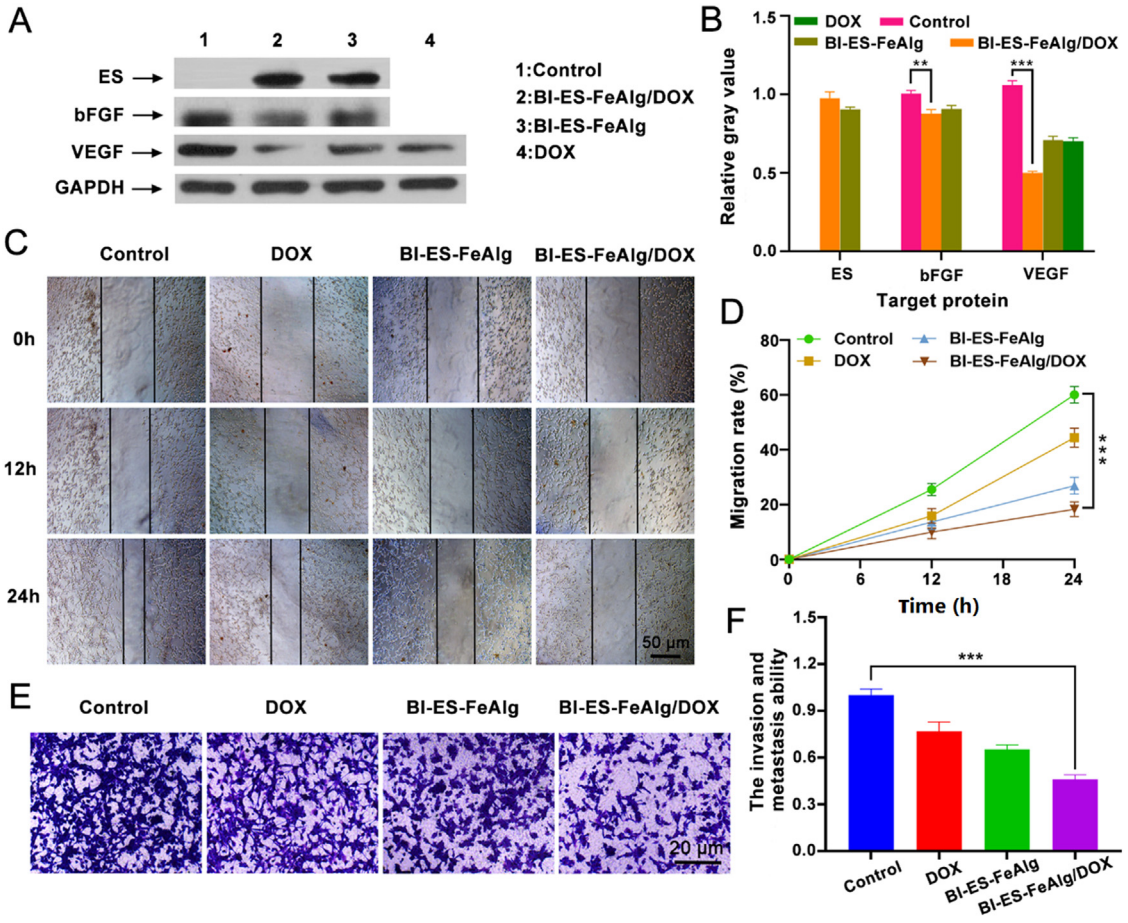

Fig. 4 – Anti-invasion and migration ability of BI-ES-FeAlg/DOX on CT-26 cells *in vitro*. (A and B) Western blot analysis of ES, bFGF and VEGF protein levels in CT-26 tumor cells after treatment with blank cell medium (Control), DOX, BI-ES-FeAlg and BI-ES-FeAlg/DOX ($n = 3$). (C) Wound healing images of Control, DOX, BI-ES-FeAlg and BI-ES-FeAlg/DOX groups at 0, 12 and 24 h. (D) Migration rates of CT-26 cells in different groups at 0, 12 and 24 h ($n = 3$). (E) Transwell assay images of CT-26 cells in Control, DOX, BI-ES-FeAlg and BI-ES-FeAlg/DOX groups. (F) The invasion and metastasis ability of CT-26 cells in Control, DOX, BI-ES-FeAlg and BI-ES-FeAlg/DOX groups ($n = 3$).

with BI-ES-FeAlg/DOX. Compared with the control group, BI-ES-FeAlg/DOX exhibited the best antitumor effect with 79.4% and 77.0% reduction in tumor numbers (Fig. 6D) and tumor load (Fig. 6E), respectively. The final tumor load in BI-ES-FeAlg/DOX group decreased from 458 to 105 mm^2. Furthermore, we tested the DAI of AOM/DSS-induced mouse model for all treatment groups to investigate the anti-tumor effect of different pharmaceutic preparations, because DAI was positively correlated with the severity of colon tumor. As seen in Fig. 6F, the DAI for Control, DOX, FeAlg, FeAlg/DOX, BI-ES-FeAlg and BI-ES-FeAlg/DOX groups was 7.17 ± 0.76, 4.33 ± 1.37, 5.00 ± 1.22, 3.17 ± 0.98, 3.40 ± 0.89 and 2.67 ± 0.82, respectively on Day 21. The lowest DAI value also proved that BI-ES-FeAlg/DOX had the most significant anti-tumor effect, and can effectively alleviate the pathological symptoms induced by orthotopic colon tumor. This dramatic anti-tumor effect of BI-ES-FeAlg/DOX was probably owing to the high-efficiency delivery of DOX, *in-situ* •OH generation property of FeAlg gel and anti-angiogenic effect of ES gene (Figs. 6G-6H and S10).

The *in vivo* biosafety of BI-ES-FeAlg/DOX was identified by blood routine index, viscera coefficient and H&E staining results. RBC and HGB are important indicators for clinical detection of anemia. As Fig. 6I showed, compared to control group, RBC and HGB in BI-ES-FeAlg/DOX group were significantly elevated, indicating that BI-ES-FeAlg/DOX can ameliorate the anemia status of mice caused by stool blood. Moreover, there was no significant difference in viscera coefficient among all treatment groups (Fig. 6J). H&E staining result (Fig. 6K) further revealed that there were no obvious pathological changes in the major organs after treatment. These results proved that BI-ES-FeAlg/DOX had good biosafety for application.

3.9. *In vivo study on CT-26 tumor-bearing mouse model*

To further verify the hypoxia targeting tropism and excellent anti-tumor performance of BI-ES-FeAlg/DOX for colon tumor, we established another CT-26 subcutaneous transplantation tumor-bearing mouse model, on which we can more directly

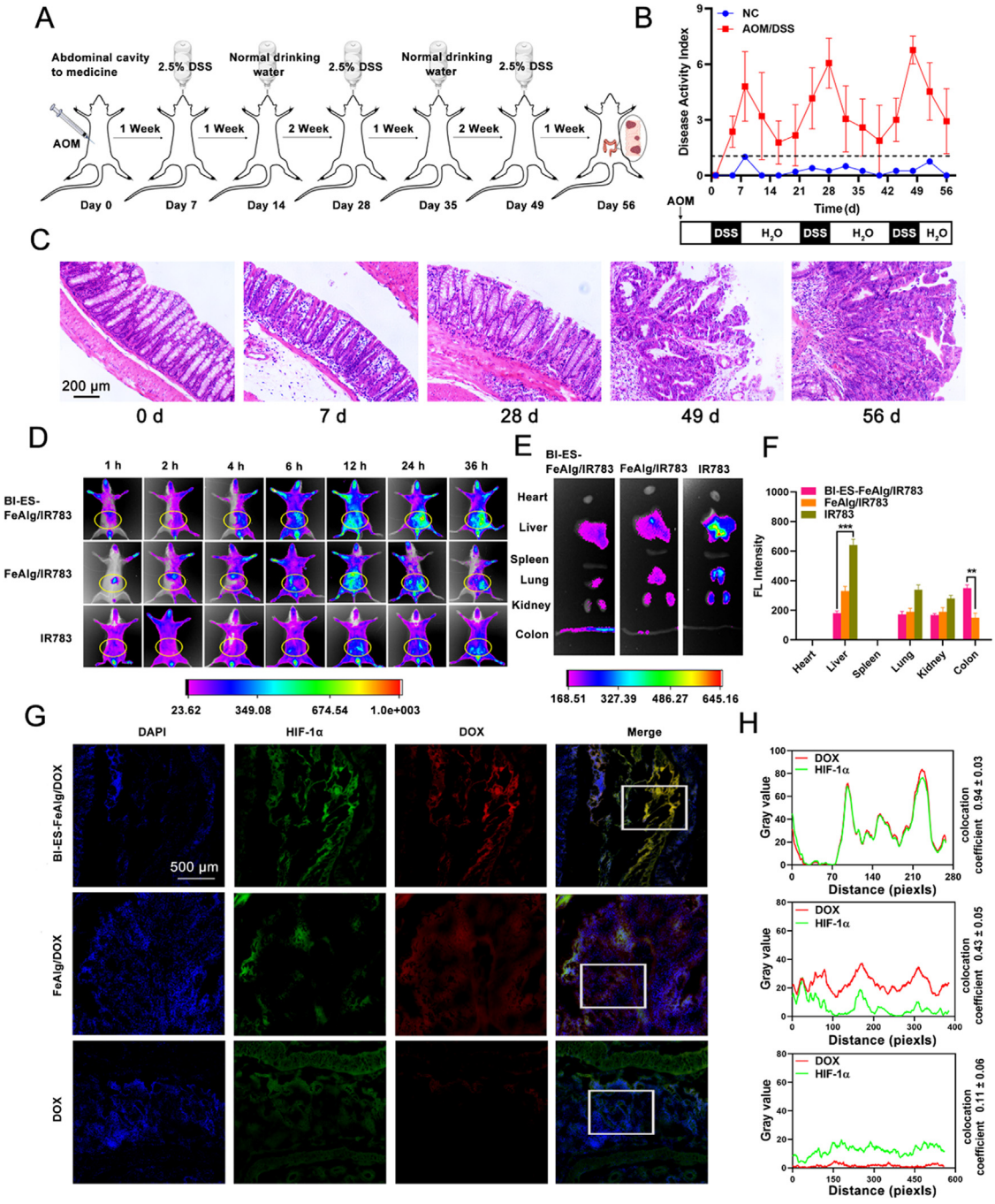

Fig. 5 – The *in vivo* tumor targeting evaluation based on hypoxia tendency on AOM/DSS model. (A) Schematic illustration of the AOM/DSS mouse model establishment. (B) The disease activity index during the AOM/DSS-induced process ($n = 6$). (C) H&E staining results of colon tissue during the AOM/DSS-induced process. (D) *In vivo* NIR imaging result to investigate the biodistribution behavior and colon tumor targeting ability of drug delivery system in AOM/DSS mouse model. The orthotopic colon tumor sites were indicated by yellow circle. (E) The *ex vivo* NIR imaging result. (F) The semiquantitative fluorescence analysis result of (E) ($n = 6$). (G) Immunofluorescence images to study the co-localization profile of DOX and hypoxic tumor region. The tumor cell and hypoxic regions were stained with DAPI (blue) and FITC-labeled HIF-1α (green), respectively. (H) The calculated colocalization coefficient of DOX and hypoxic tumor regions. The white square frame represented the analysis areas.

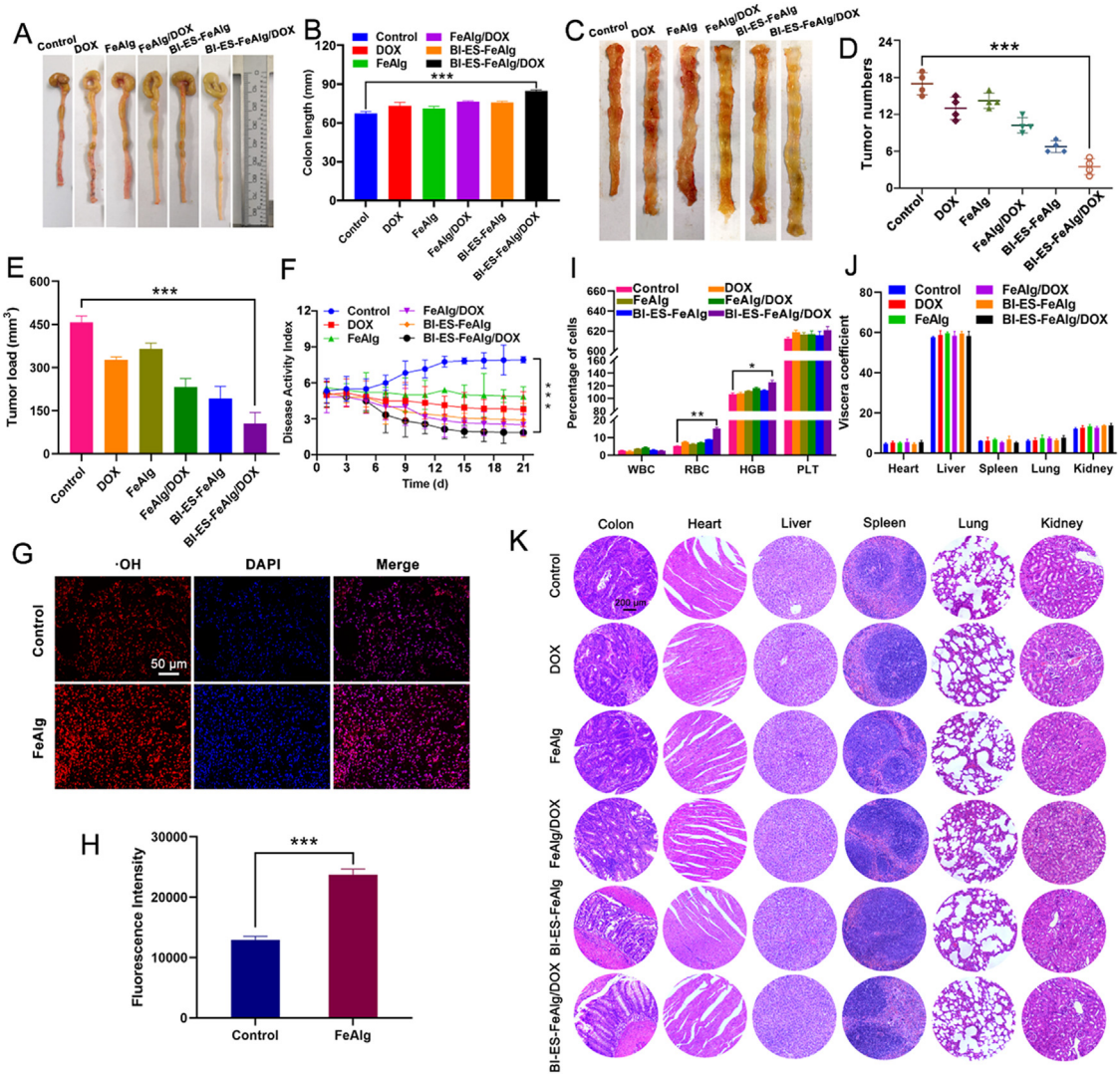

Fig. 6 – *In vivo* anti-tumor efficacy on AOM/DSS mouse model. (A) Image of colon morphology and length of each treatment group. (B) Quantitative analysis of colon length in each group after treatment ($n = 6$). (C) The longitudinal-section image of colon tissues in each group after treatment. (D) Quantitative analysis of tumor numbers per colon tissue in different treatment groups ($n = 6$). (E) The calculated tumor load per colon tissue in different treatment groups ($n = 6$). (F) The disease activity index (DAI) of mice ($n = 6$). (G and H) The ·OH level in colon tumor ($n = 6$). (I) The blood routine index (including WBC, RBC, HGB and PLT) of mice in different treatment groups ($n = 6$). (J) The viscera coefficient of mice in different treatment groups ($n = 6$). Viscera coefficient = Weight of organs (mg)/ Weight of mouse (g). (K) H&E results of different treatment groups.

and easily observe the targeting effect and changes in tumor volume during treatment. As shown in Fig. 7A, CT-26 colon tumor cells were injected subcutaneously into the right forelimb of mice, and one week later, this model was used for subsequent *in vivo* studies. Real-time biodistribution result (Fig. 7B) demonstrated that free IR783 and FeAlg/IR783 groups exhibited weak fluorescence signals in tumor tissues, while BI-ES-FeAlg/IR783 group showed strong and long-term fluorescence signal in tumors. In addition, Fig. 7C-7D demonstrated free IR783 mainly distributed in liver tissue, while BI-ES-FeAlg/IR783 primarily existed in tumor tissue. It was particularly noteworthy that the fluorescence of BI-ES-FeAlg/IR783 was mainly concentrated in the hypoxic central area of the tumor tissue. This may be attributed to the hypoxic biological tendency of BI.

Moreover, in order to investigate the effect of FeAlg gel coating on the circulation time of BI-ES *in vivo*, pharmacokinetic experiment was carried out. As Fig. S11 shown, the colonies of blood sample taken from BI-ES-FeAlg/DOX treated mice at 24 h and 36 h were around 5 and 10 times greater than that of uncoated BI-ES, respectively. This indicated that FeAlg gel coating on the surface of BI-ES had a certain protective effect and reduced the clearance of BI bacteria in the body, thus providing more effective retention in blood circulation. In addition, to further explore the reason for this phenomenon, the cytokines (IL-10 and TNF-α) associated with BI immunogenicity was measured. As Fig. S12 shown, the levels of IL-10 and TNF-α in BI-ES-FeAlg/DOX group were both significantly lower than that of BI-ES group, suggesting that FeAlg gel coating on the surface of

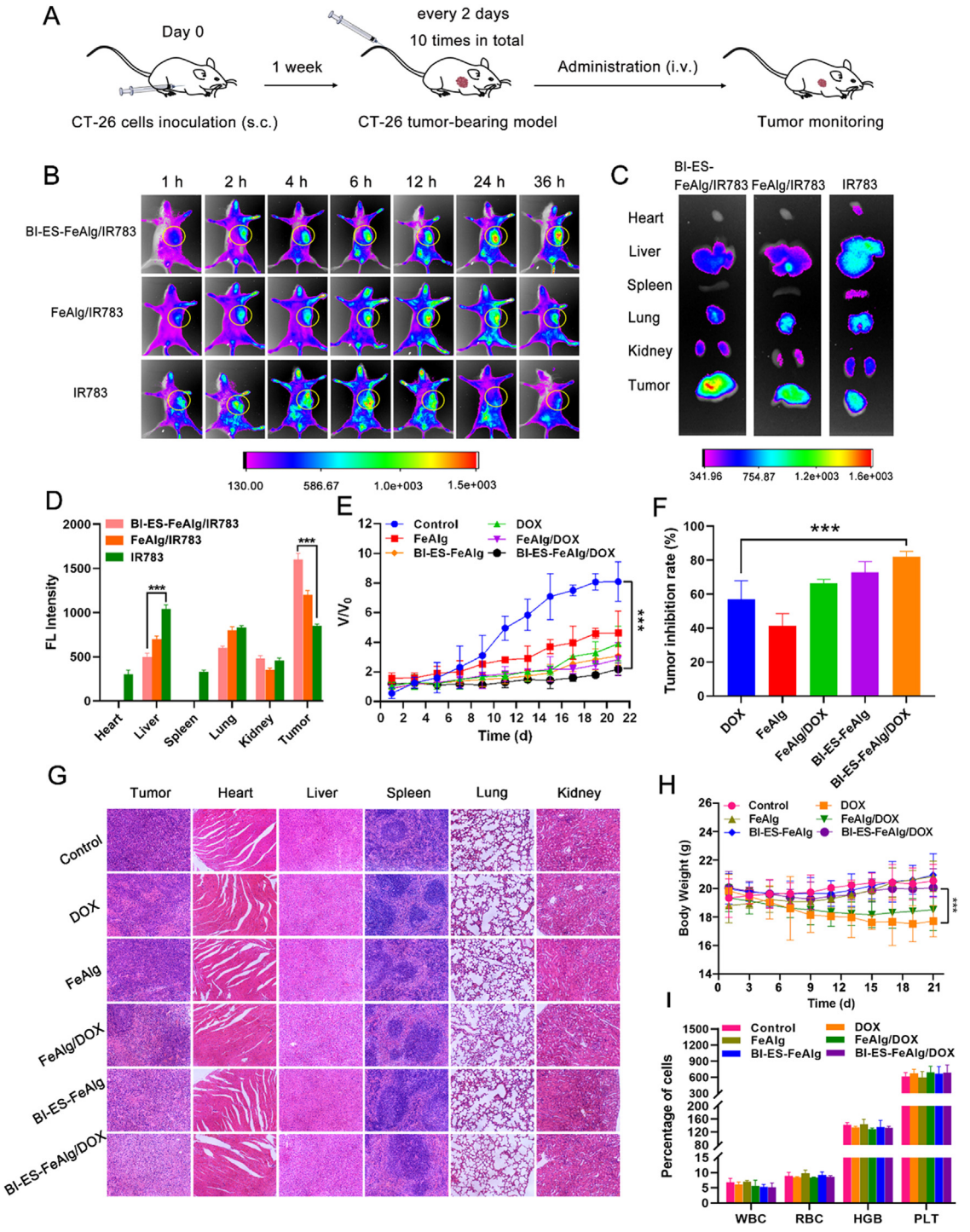

Fig. 7 – Biodistribution, anti-tumor effect and safety evaluation on CT-26 tumor-bearing model. (A) Schematic illustration of mouse model establishment and BI-ES-FeAlg/DOX therapy. (B) *In vivo* NIR imaging result to investigate the biodistribution behavior and tumor targeting ability of drug delivery system. The colon tumor sites were indicated by yellow circle.(C) The *ex vivo* NIR imaging result. (D) The semiquantitative fluorescence analysis result of (C) ($n = 6$). (E) Trend chart of relative tumor volume with treatment time ($n = 6$). (F) The tumor inhibition rate of different treatment groups ($n = 6$). (G) H&E staining results of tumor tissue and major organs. (H) Body weight change of CT-26 tumor-bearing mice during treatment period ($n = 6$). (I) The blood routine index of mice in each group after treatment ($n = 6$).

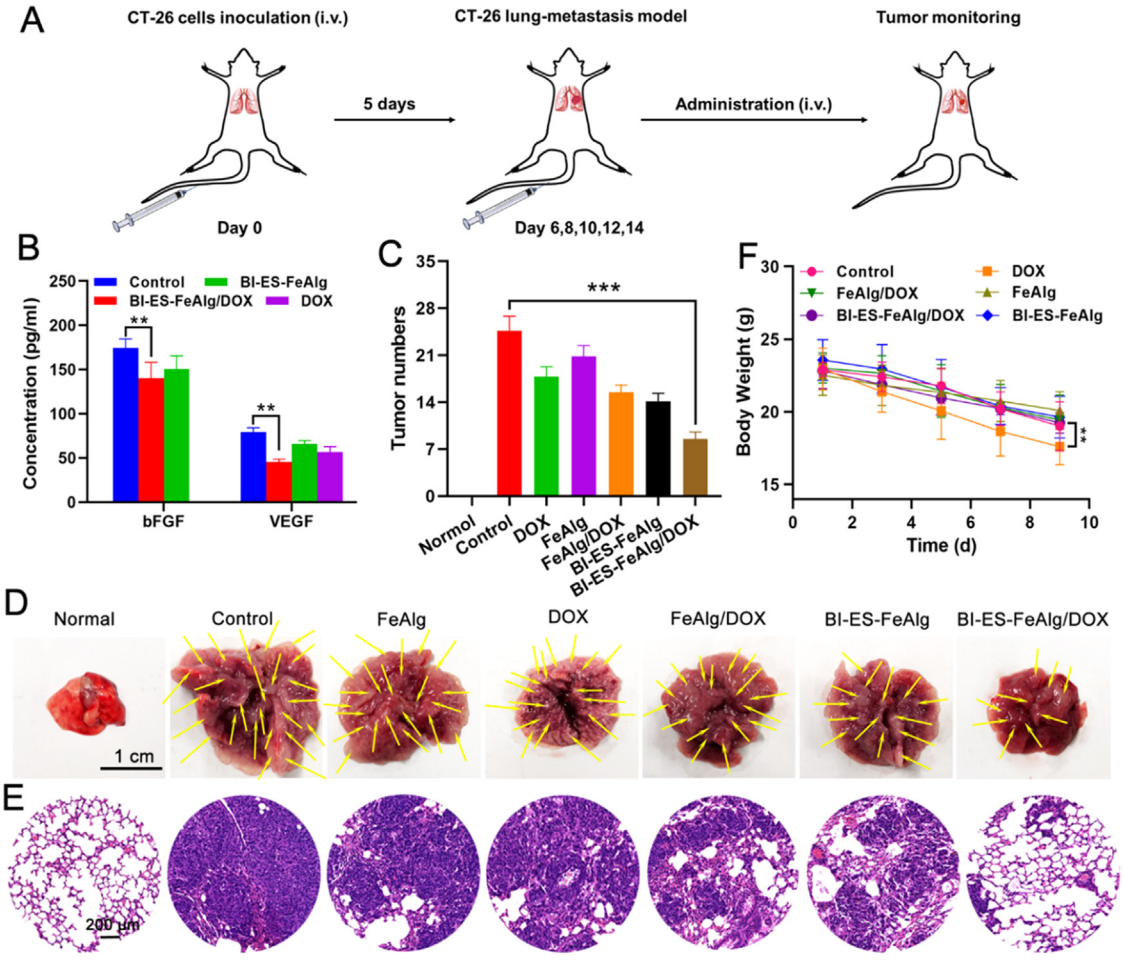

Fig. 8 – Anti-lung metastasis effect *in vivo*. (A) Schematic illustration of CT-26 lung-metastasis model establishment and BI-ES-FeAlg/DOX therapy. (B) The VEGF and bFGF protein levels in lung tissue of different groups ($n = 6$). (C) The number of tumor nodules in lung tissues ($n = 6$). (D) Images of lung tissues in the different treatment groups. The tumor nodules are indicated by yellow arrows. (E) H&E staining results of lung tissues. (F) Body weight change of CT-26 lung-metastasis mice during the administration period ($n = 6$).

BI-ES can reduce the immunogenicity of BI bacteria, thereby reducing phagocytosis of bacteria by the RES system and prolonging the circulation time in the body. This is because Alg has good biocompatibility and low immunogenicity. FeAlg coating can mask the surface antigens of BI-ES, to reduce the immunogenicity of BI bacteria.

Fig 7B-7D showed that BI-ES-FeAlg/IR783 group exhibited a stronger fluorescence signal in the tumor region even a relatively long period (36 h) after administration. Based on the above results, it can be inferred that this excellent tumor retention capacity could not be attributed to its tumor targeting ability but also to its long *in vivo* circulation time. This also provided a guarantee for better exertion of anti-tumor effect *in vivo*.

Then the antitumor effect was evaluated as shown in Fig.7A. The trend of relative tumor volume in each group over time was shown in Fig. 7E. Compared with the highest V/V_0 of 8.10 ± 1.34 in PBS control group, BI-ES-FeAlg/DOX contributed to a prominent antitumor effect with the lowest V/V_0 of 2.19 ± 0.41. Furthermore, the tumor inhibition rate was calculated based on the final tumor weight. As exhibited in Fig. 7F and S13, BI-ES-FeAlg/DOX group showed the smallest tumor size, as well as the highest tumor inhibition rate of 82.12% ± 3.08%. In addition, H&E staining result of tumor tissues (Fig. 7G) revealed that a large amount of tumor cells exhibited necrosis after treatment with BI-ES-FeAlg/DOX, further suggesting the greatest therapeutic efficacy of BI-ES-FeAlg/DOX.

Finally, the systemic toxicity of BI-ES-FeAlg/DOX was evaluated. Fig. 7H showed that in DOX and FeAlg/DOX groups, the weight of mice decreased obviously over time, while in BI-ES-FeAlg/DOX group, there was no significant decline in body weight. Moreover, the levels of blood routine index, such as WBC, RBC, HGB and PLT, were all in the normal ranges (Fig. 7I), indicating no obvious hematologic toxicity. H&E result (Fig. 7G) further proved that there were no pathological changes in the major organs after BI-ES-FeAlg/DOX treatment.

3.10. *Anti-metastatic effect study in vivo*

CT-26 tumor has a high degree of malignancy and is prone to lung-metastases and liver-metastases. Herein, we constructed

a CT-26 lung metastasis model to evaluate the anti-metastatic effect of BI-ES-FeAlg/DOX *in vivo* (Fig. 8A). Elisa analysis was performed to determine the bFGF and VEGF downregulation effects of BI-ES-FeAlg/DOX (Figs. S14 and S15). As shown in Fig. 8B, compared to PBS control group, BI-ES-FeAlg and BI-ES-FeAlg/DOX both showed downregulation effect on bFGF and VEGF proteins, suggesting that ES gene can competitively inhibit bFGF and VEGF expression. What's noteworthy was that in BI-ES-FeAlg/DOX group, the synergistic effect of ES and DOX could exhibit downregulation of VEGF protein significantly, which was in accordance with western blot results *in vitro*.

As we know, downregulation of bFGF and VEGF proteins is beneficial to block tumor angiogenesis and inhibit tumor metastasis. Therefore, we further studied the anti-metastatic effect of BI-ES-FeAlg/DOX on CT-26 lung metastasis mouse model. As shown in Fig. 8C-8D, the pulmonary tumor nodules in BI-ES-FeAlg group (14.17 ± 1.17) were significantly less than those of PBS control group (24.67 ± 2.16). There were only 8.50 ± 1.05 pulmonary tumor nodules in BI-ES-FeAlg/DOX group. Moreover, in PBS control group, the lungs were enlarged with rough surface due to the severe tumor infiltration. While in BI-ES-FeAlg/DOX group, the lung size tended to be normal with relatively smooth surface because of the excellent anti-tumor metastasis effect. In addition, Fig. 8E showed that metastatic tumor cells in lung tissue of PBS control group were closely arranged, and the alveolar structure basically disappeared. However, after BI-ES-FeAlg/DOX treatment, there were only relatively few tumor cells appearing in lung tissue with clear and complete alveolar structure. All above results indicated that BI-ES-FeAlg/DOX could effectively inhibit the lung metastasis of CT-26 tumor cells *in vivo*. What's more, compared with the control group, the body weight of the mice after BI-ES-FeAlg/DOX treatment did not decrease significantly (Fig. 8F), suggesting the low systemic toxicity of BI-ES-FeAlg/DOX [38].

4. Conclusion

In this study, a self-guidance biological hybrid drug delivery system (BI-ES-FeAlg/DOX) driven by anaerobes BI was successfully constructed to inhibit the proliferation and metastasis of colon tumor. *In vitro* and *in vivo* results proved that attributed to the hypoxic biological tendency of BI, BI-ES-FeAlg/DOX can efficiently deliver ES gene and chemotherapeutic drug DOX into the hypoxic tumor targets. After arrived at colon tumor tissue, DOX can be selectively released under the condition of low pH and high GSH in TME. In addition, FeAlg catalyzed H_2O_2 in the local tumor to generate cytotoxic ·OH, further enhancing the antitumor effect. Meanwhile, BI-ES colonized tumor locally and expressed ES gene, to block angiogenesis and inhibit colon tumor metastasis by down-regulating bFGF, as well as cooperating with DOX to down-regulate VEGF expression. These results indicated that the BI-based biological hybrid drug delivery system offered a potential and innovative drug delivery strategy to overcome the biological transport barriers and realize combined delivery of gene and chemotherapeutic drugs in a TME-sensitive manner.

Conflicts of Interest

The authors declare no conflict of interest.

Acknowledgments

This work was supported by National Natural Science Foundation of China (82102918) and Youth Talent Promotion Project in Henan Province (2020HYTP011).

Supplementary materials

Supplementary material associated with this article can be found, in the online version, at doi:10.1016/j.ajps.2022.09.003.

REFERENCES

[1] Sung H, Ferlay J, Siegel RL, Laversanne M, Soerjomataram I, Jemal A, et al. Global cancer statistics 2020: GLOBOCAN estimates of incidence and mortality worldwide for 36 cancers in 185 countries. CA Cancer J Clin 2021;0:1–41.
[2] Bergers G, Fendt SM. The metabolism of cancer cells during metastasis. Nat Rev Cancer 2021;21(3):162–80.
[3] Engstrand J, Nilsson H, Stromberg C, Jonas E, Freedman J. Colorectal cancer liver metastases - a population-based study on incidence, management and survival. BMC Cancer 2018;18(1):78.
[4] Riihimäki M, Hemminki A, Sundquist J, Hemminki K. Patterns of metastasis in colon and rectal cancer. Sci Rep 2016;6:29765.
[5] Wyld L, Audisio RA, Poston GJ. The evolution of cancer surgery and future perspectives. Nat Rev Clin Oncol 2015;12(2):115–24.
[6] Allen BM, Iam HKJ, Burnett CE, Venida A, Spitzer MH. Systemic dysfunction and plasticity of the immune macroenvironment in cancer models. Nat. Med. 2020;26(7):1125–34.
[7] Taieb J, Lapeyre-Prost A, Puig PL, Zaanan A. Exploring the best treatment options for BRAF-mutant metastatic colon cancer. Br J Cancer 2019;121(6):434–42.
[8] Dawson JC, Serrels A, Stupack DG, Schlaepfer DD, Frame MC. Targeting FAK in anticancer combination therapies. Nat Rev Cancer 2021;24:1–12.
[9] Dong X, Liu HJ, Feng HY, Yang SC, Liu XL, Lai X, et al. Enhanced drug delivery by nanoscale integration of a nitric oxide donor to induce tumor collagen depletion. Nano Lett 2019;19(2):997–1008.
[10] Sun MC, Yang SH, Huang HW, Gao P, Pan SW, Cheng ZG, et al. Boarding oncolytic viruses onto tumor-homing bacterium-vessels for augmented cancer immunotherapy. Nano Lett 2022;22(12):5055–64.
[11] Lou X, Chen Z, He Z, Sun M, Sun J. Bacteria-mediated synergistic cancer therapy: small microbiome has a big hope. Nanomicro Lett 2021;13(1):37.
[12] Cao ZP, Liu JY. Bacteria and bacterial derivatives as drug carriers for cancer therapy. J Control Release 2020;326:396–407.
[13] Sun M, Ye H, Shi Q, Xie J, Yu X, Ling H, et al. Both-in-one hybrid bacteria suppress the tumor metastasis and relapse via tandem-amplifying reactive oxygen species-immunity responses. Adv Healthc Mater 2021;10(21):e2100950.

[14] Skelly AN, Sato Y, Kearney S, Honda K. Mining the microbiota for microbial and metabolite-based immunotherapies. Nat Rev Immunol 2019;19(5):305–23.
[15] Swanson KS, Gibson GR, Hutkins R, Reimer RA, Reid G, Verbeke K, et al. The international scientific association for probiotics and prebiotics (ISAPP) consensus statement on the definition and scope of synbiotics. Nat Rev Gastro Hepat 2020;17(11):687–701.
[16] Routy B, Gopalakrishnan V, Daillere R, Zitvogel L, Wargo JA, Kroemer G. The gut microbiota influences anticancer immunosurveillance and general health. Nat Rev Clin Oncol 2018;15(6):382–96.
[17] Zuo F, Zeng Z, Hammarstrm L, Marcotte H. Inducible plasmid self-destruction (IPSD) assisted genome engineering in lactobacilli and Bifidobacteria. ACS Synth Biol 2019;8(8):1723–9.
[18] Mavrich TN, Casey E, Oliveira J, Bottacini F, James K, Franz CMAP, et al. Characterization and induction of prophages in human gut-associated Bifidobacterium hosts. Sci Rep 2018;8:1–17.
[19] Wang L, Vuletic I, Deng D, Crielaard W, Xie Z, Zhou K, et al. Bifidobacterium breve as a delivery vector of IL-24 gene therapy for head and neck squamous cell carcinoma *in vivo*. Gene Ther 2017;24(11):699–705.
[20] Zhu H, Li Z, Mao S, Ma B, Zhou S, Deng L, et al. Antitumor effect of sFlt-1 gene therapy system mediated by Bifidobacterium Infantis on Lewis lung cancer in mice. Cancer Gene Ther 2011;18(12):884–96.
[21] Franses JW, Baker AB, Chitalia VC, Edelman ER. Stromal endothelial cells directly influence cancer progression. Sci Transl Med 2011;3(66):66ra5.
[22] Cao YH, Langer R. Optimizing the delivery of cancer drugs that block angiogenesis. Sci Transl Med 2010;2(15):15ps3.
[23] Marx J. Cancer-encouraging results for second-generation antiangiogenesis drugs. Science 2005;308(5726):1248–9.
[24] Feldman AL, Libutti SK. Progress in antiangiogenic gene therapy of cancer. Cancer 2000;89(6):1181–94.
[25] Abdollahi A, Hahnfeldt P, Maercker C, Grne HJ, Huber PE. Endostatin's antiangiogenic signaling network. Mol Cell 2004;13(5):649–63.
[26] Liang K, Liu Q, Li P, Han Y, Bian XP, Tang YB, et al. Endostatin gene therapy delivered by attenuated Salmonella typhimurium in murine tumor models. Cancer Gene Ther 2018;25(7–8):167–83.
[27] Ma Y, Bao DM, Zhang JJ, Jin XB, Wang J, Wang Y, et al. Antitumor activities of Liver-targeting peptide modified recombinant human endostatin in BALB/c-nu mice with Hepatocellular carcinoma. Sci Rep 2017;7:14074.
[28] Yu Y, Wang YY, Wang YQ, Wang X, Liu YY, Wang JT, et al. Antiangiogenic therapy using endostatin increases the number of ALDH plus lung cancer stem cells by generating intratumor hypoxia. Sci Rep 2016;6:34239.
[29] Dang LH, Bettegowda C, Agrawal N, Cheong I, Huso D, Frost P, et al. Targeting vascular and avascular compartments of tumors with C. novyi-NT and anti-microtubule agents. Cancer Biol Ther 2004;3(3):326–37.
[30] Liu FJ, Tan G, Li J, Dong XS, Krissansen GW, Sun XY. Gene transfer of endostatin enhances the efficacy of doxorubicin to suppress human hepatocellular carcinomas in mice. Cancer Sci 2007;98(9):1381–7.
[31] Hu B, Kou L, Li C, Zhu LP, Fan YR, Wu ZW, et al. Bifidobacterium longum as a delivery system of TRAIL and endostatin cooperates with chemotherapeutic drugs to inhibit hypoxic tumor growth. Cancer Gene Ther 2009;16(8):655–63.
[32] Zhang H, Qu H, Chen J, Li M, Du H, Hou L, et al. Construction and research on size and phase 'fixed-point remodelling' intelligent drug delivery system. J Drug Target 2021;29(1):108–20.
[33] Zhang H, Ren Y, Hou L, Chang J, Zhang Z, Zhang H. Positioning remodeling nanogels mediated codelivery of antivascular drug and autophagy inhibitor for cooperative tumor therapy. ACS Appl Mater Interfaces 2020;12(6):6978–90.
[34] Rossi M, Brigidi P, Matteuzzi D. An efficient transformation system for Bifidobacterium spp. Lett Appl Microbiol 1997;24(1):33–6.
[35] Drozdz M, Makuch S, Cieniuch G, Wozniak M, Ziolkowski P. Obligate and facultative anaerobic bacteria in targeted cancer therapy: current strategies and clinical applications. Life Sci 2020;261:118296.
[36] Tanaka T, Kohno H, Suzuki R, Yamada Y, Sugie S, Mori H. A novel inflammation-related mouse colon carcinogenesis model induced by azoxymethane and dextran sodium sulfate. Cancer Sci 2010;94(11):965–73.
[37] Yang HX, Wang WC, Romano KA, Gu M, Sanidad KZ, Kim D, et al. A common antimicrobial additive increases colonic inflammation and colitis-associated colon tumorigenesis in mice. Sci Transl Med 2018;10(443):eaan4116.
[38] Hou L, Gong X, Yang J, Zhang HJ, Yang WJ, Chen XY. Hybrid-Membrane-Decorated Prussian Blue for Effective Cancer Immunotherapy via Tumor-Associated Macrophages Polarization and Hypoxia Relief. Adv Mater 2022;34(14):2200389.